Journal of Catalysis **200,** 117–130 (2001)
doi:10.1006/jcat.2001.3193, available online at http://www.idealibrary.com on IDEAL®

Supported CuO + Ag/Partially Stabilized Zirconia Catalysts for the Selective Catalytic Reduction of NO_x under Lean Burn Conditions

1. Bulk and Surface Properties of the Catalysts

Vladislav A. Sadykov,*,†,[1] R. V. Bunina,* G. M. Alikina,* A. S. Ivanova,* D. I. Kochubei,* B. N. Novgorodov,* E. A. Paukshtis,*,† V. B. Fenelonov,* V. I. Zaikovskii,* T. G. Kuznetsova,* S. A. Beloshapkin,*,† V. N. Kolomiichuk,* E. M. Moroz,* V. A. Matyshak,‡ G. A. Konin,‡ A. Ya. Rozovskii,§ J. R. H. Ross,¶ and J. P. Breen¶

*Boreskov Institute of Catalysis, Siberian Branch of the Russian Academy of Sciences, Lavrentieva 5, Novosibirsk 630090, Russia; †Novosibirsk State University, Pirogova 1, Novosibirsk 630090, Russia; ‡Semenov Institute of Chemical Physics RAS, Moscow, Russia; §Topchiev Institute of Petrochemical Synthesis RAS, Moscow, Russia; and ¶University of Limerick, Limerick, Ireland

Received October 6, 2000; revised January 30, 2001; accepted February 2, 2001; published online April 11, 2001

Thermally stable cubic mesoporous zirconia samples stabilized by the alkaline-earth cations (Ca, Sr, Ba) were synthesized via the coprecipitation route followed by refluxing in the presence of surfactants. These systems were used as supports for copper cations and then modified by the addition of silver nanoparticles using impregnation or photoassisted deposition techniques. The structural, textural, and surface features of these nanosystems were studied by using TEM, X-ray diffraction, EXAFS, nitrogen adsorption isotherms, SAXS, FTIRS of adsorbed CO, and TPD of adsorbed NO_x species. Partially stabilized zirconia samples were found to possess a disordered cubic structure. A higher tendency of bulky Ba cation to segregate in the surface layer is reflected in a higher degree of surface disordering, higher concentration of hydroxyls, and greater coordination unsaturation of isolated copper cations. In contrast to such traditional supports as γ-alumina, stabilized zirconia supports appear to favor formation of small reactive (probably, three-dimensional) clusters of copper cations possessing an increased reactivity and decreased strength of oxygen bonding with these cations. It is reflected in decreased thermal stability of surface nitrite and nitrate species located at these centers as compared with such species on the surface of CuO/alumina catalysts. This feature seems to be primarily determined by the specificity of the surface structure of fluorite-like supports (ceria, zirconia). Silver incorporation into copper oxidic clusters decreases the strength of copper–oxygen bonds as well as the thermal stability of adsorbed nitrite–nitrate species. For samples prepared via the photodeposition route, the clustering degree of copper cations is usually lower than in the case of samples obtained by traditional impregnation procedure.

Key Words: **partially stabilized zirconia; mesoporosity; synthesis; supported copper oxide; silver; characterization; bulk and surface structure; adsorption properties; NO_x; CO.**

[1] To whom correspondence should be addressed at Boreskov Institute of Catalysis, Siberian Branch of the Russian Academy of Sciences, Lavrentieva 5, Novosibirsk Russia 630090. Fax: (7-3832) 343-056. E-mail: sadykov@catalysis.nsk.su.

INTRODUCTION

Zirconia-supported transition metal cations are known to possess a reasonably good catalytic activity in the reactions of NO_x-selective reduction by hydrocarbons in the excess of oxygen (NO_x HC-SCR) (1–6). Among these systems, CuO/ZrO_2 or Cu/sulfated ZrO_2 appear to have a remarkable low-temperature (in the range of 200–300°C) activity compared with or exceeding that of Cu-ZSM-5, while being much more stable hydrothermally. This activity was usually assigned to a high number of isolated Cu cations stabilized by these supports, while CuO crystallites emerging at high copper loadings are thought to be either inactive or nonselective. However, as was indicated in [7], small copper oxidic clusters epitaxially bound with support could also be of importance. Another attractive feature of these systems, when compared with Cu-ZSM-5, is their hydrothermal stability and mesoporosity; the latter allows the use of long-chain hydrocarbon reductants. However, as a rule, zirconias used as supports are either monoclinic samples with relatively low surface area or sulfated tetragonal modifications. In the former case, the disadvantage of such supports is obvious, while in the latter, low stability of surface sulfates in the hydrothermal conditions of real exhausts could be a problem. Earlier (8), highly dispersed tetragonal and/or cubic modifications of ZrO_2 partially stabilized by alkaline-earth cations were synthesized and shown to be rather active in the high-temperature (500–600°C) NO_x reduction by propane in the excess of oxygen. This paper aims at using this approach for preparation of high-surface-area stabilized zirconia supports. Moreover, refluxing in the presence of surfactants (9) was applied to ensure the mesoporosity of supports and their high-temperature stability. Supported copper oxidic species known for their reasonable middle-temperature performance in NO_x HC-SCR were chosen here as the

0021-9517/01 $35.00

active component. To improve the low-temperature activity of CuO/stabilized zirconia systems, by analogy with approaches used earlier for alumina [10] and Ce-ZSM-5 catalysts [11], silver was added. To understand the factors determining performance of supported copper systems in the reactions of NO_x reduction by hydrocarbons, their bulk and surface properties were studied by using a combination of structural and spectroscopic methods (TEM, X-ray diffraction, EXAFS, nitrogen adsorption isotherms, SAXS, FTIRS of adsorbed CO, and TPD of adsorbed NO_x species). For comparison, a Cu (+ Ag)/alumina catalyst was also studied.

METHODS

Bulk samples of highly dispersed mesoporous ZrO_2 partially stabilized by Ca, Sr, and Ba were prepared by coprecipitation of the corresponding mixed nitrate solutions with ammonia, surfactants (up to 1 wt% of polyvinyl alcohol or polyethylene oxide) were also added, followed by refluxing for 120 h. After filtration, samples were washed by distilled water until all nitrates were removed and then washed with ethanol, dried at 110°C for 14 h, and calcined for 4 h in a stream of air at 600°C.

For comparison, as a traditional support, the earlier studied commercial γ-Al_2O_2 sample (A-1 type) with the specific surface area ~180 m^2/g (12) was used.

To support the active components, three types of procedures were used. In the first one, copper (up to 5 wt%), was supported on the surface of zirconia or alumina from the nitrate solutions by a standard wet impregnation procedure followed by drying for 6 h at 120°C (periodically grinding zirconia-supported sample with a pestle and mortar) and calcination at 400°C for 4 h. To add up to 2 wt% of silver, a sample with supported copper was impregnated by the silver nitrate solution of a required concentration. The drying and calcination procedures were the same as described above, with a final calcination at 400°C for 2 h. To ensure a homogeneous distribution of silver, the calcined CuO + Ag/ZrO_2 samples were ground and wetted with ca 15 wt% HNO_3 solution. After thorough mixing, samples were dried and calcined as described above.

In the second method, copper and then silver were added to supports by mixing the support with copper acetate (pH 5.4) or silver nitrate (pH 6.3) solutions and then purging with Ar under illumination by a high-pressure DRL-250 mercury lamp for 1.5 h (Cu) and 10 min (Ag), respectively. After photodeposition, samples were washed by distilled water, dried under an IR lamp for 5 h, and calcined at 400°C for 2 h.

The third procedure was used to support a small amount of copper cations in a manner similar to that applied for the cation exchange in zeolites (12). In this case, a powder of zirconia support was placed into 0.15 M copper nitrate solution and kept stirring at 80°C for 2 h and then filtered, dried, and calcined at 500°C for 4 h. The copper content was found to be close to 0.2 wt% for all supports.

The chemical composition of samples was analyzed by the atomic absorption spectroscopy (a Karl Zeiss Jena AAS1N spectrometer). The X-ray phase analysis was carried out by using a HZG-4C diffractometer with monochromatized Cu$K\alpha$ radiation. The unit cell parameter of partially stabilized zirconia was determined from the positions of 222 and 311 diffraction peaks of the doubled unit cell (vide infra). The accuracy of the unit size determination ($\sim\pm 3 \times 10^{-3}$ Å) was estimated from comparison with results obtained for the International X-ray standard corundum sample. The apparent particle sizes (D) were estimated by the Scherrer equation. Adsorption characteristics were measured on a Micromeritics ASAP-2400 installation by N_2 adsorption at ~77 K.

EXAFS spectra of the K-edge of Zr and Cu X-ray absorption were obtained at the EXAFS Station of the Siberian Center of Synchrotron Radiation, Novosibirsk. The storage ring VEPP-3 with the electron beam energy 2GeV and a typical filled current of 70 mA was used as the radiation source. The energy of the X-ray quanta was monitored with the help of the cutoff Si (111) monochromator. X-ray absorption spectra were recorded at room temperature in the transmission mode using two ionization chambers, i.e., the monitoring one and the full absorption one. Sample powders were mixed with the Apiezon T grease, and spectra were collected at room temperature. The thickness of samples was chosen to achieve the optimal absorption jump.

The X-ray absorption data were analyzed for interval of the wave numbers k from 3.0 to 15.0 $Å^{-1}$ for Zr spectra and 3.0–11. $Å^{-1}$ for those of Cu in the form of $k^3\chi(k)$, where $\chi(k)$ is the oscillating part of the absorption coefficient μ. The background was removed by extrapolating absorption in the pre-edge region onto the EXAFS region in the form of Victoreen's polynomials. Three cubic splines were used to construct the smooth part of μ. The inflection point of the edge of the X-ray absorption spectrum was used as the initial point ($k = 0$) of the EXAFS spectrum. The curve-fitting with the help of EXCURV-92 procedure was used to determine the interatomic distances and coordination numbers from the EXAFS spectra.

Samples were also characterized using TEM (JEM 2010, 200 kV) and X-ray small angle scattering (SAXS, a KRM-1 camera with CuK_α radiation, nickel filter, and an amplitude analyzer). Surface properties were probed by the Fourier transform infrared spectroscopy (FTIRS) of adsorbed CO (IFS 113V Bruker spectrometer). In those experiments, samples were pressed in wafers with densities 4.4–22.7 mg/cm^2 and pretreated in the IR cell first at 100 Torr of O_2 and then in vacuum at 400°C for 1 h. CO was adsorbed at 77 K first by introducing several doses (each

CO dose corresponds to ~4 μmol), finally setting CO pressure to 10 Torr. By using a routine computer processing, the data were presented as absorbance normalized to the unit weight of sample, which allows one to directly compare results obtained for different samples.

The temperature-programmed desorption of NO_x (TPD) from the surface of samples after oxidative pretreatment was carried out with the temperature ramp from 25 to 550°C at 10°C/min rate using a chemiluminescence NO_x Beckman analyzer and following procedures described earlier in detail (12). For the systems studied here subjected to the oxidative pretreatment, no evolution of nitrous oxide was detected in TPD runs, which was checked by using a Perkin Elmer "Spectrum RX I FT-IR" system and a gas cell.

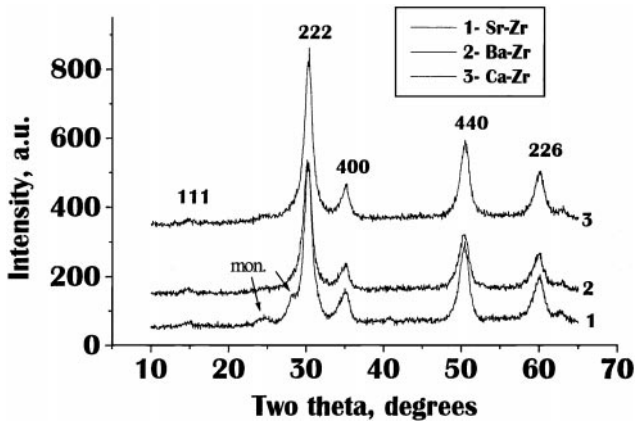

FIG. 1. Typical X-ray diffraction data for mesoporous partially stabilized zirconia supports.

RESULTS

1. Structural and Textural Features of Stabilized Zirconia Supports

Phase composition and structural parameters. X-ray data presented in Fig. 1 and in Table 1 indicate that despite the low content of stabilizing cations, samples annealed at 600°C possess a cubic structure with a small admixture of the monoclinic phase for Sr-modified sample. In this respect, samples refluxed in the presence of surfactants differ from those calcined without refluxing: in the latter case, at this content of stabilizing cation, the structure is either monoclinic or tetragonal [8]. Another important feature of samples synthesized in this work is their rather good crystallinity, which is reflected in the presence of a set of strong peaks in the diffraction pattern. The presence of a superstructural peak at $2\Theta \sim 15°$, i.e., at a position exactly matching a half of that for the intense 222 peak situated at $2\Theta \sim 30°$, indicates a doubling of the zirconia unit cell via some ordering of the oxygen vacancies created due to the presence of guest Me^{2+} cations in the lattice. The doubled unit cell size systematically increases with the increase of the guest cation radius in the order Ca < Sr < Ba. The apparent particle sizes estimated from the broadening of 226 peak decline in the order Ca > Sr > Ba (Table 1). In fact, microstrains are in part responsible for the peak broadening as well, as follows from comparison of the 222 and 226 peaks widths. Indeed, the ratio of the half-widths of these peaks ($\beta_{226}/\beta_{222} = 1.3$) somewhat differs from the value corresponding to the reciprocal ratio of the reflection angles cosines (1.1), which is to be observed in the case of a pure size broadening effect. However, the experimental ratio differs strongly from the value predicted in the case of broadening caused by microstrains (2.15), thus implying a relatively small density of those defects.

Typical EXAFS spectra for ZrK edge are shown in Fig. 2, while corresponding structural parameters are presented in Table 2. In all samples, the Zr environment corresponds to that of the disordered cubic zirconia phase. Here, a set of close Zr–O distances exists, thus decreasing the average Zr–O coordination number (CN). Though in the first approximation the nature of the guest cation has a small effect on the Zr coordination sphere, Ca-modified samples appear to be more ordered when compared with the other two systems.

Textural properties. Figure 3 illustrates typical TEM data for stabilized zirconia samples. Small sizes of particles revealed by TEM agree with those estimated from the X-ray data. High dispersion of stabilized zirconia supports is confirmed by the nitrogen adsorption measurements

TABLE 1

Structural and Textural Data for Stabilized Zirconia Supports Annealed at 600°C

		X-ray data		Textural data			
Type of guest cation (M)	MO content (mol%)	Unit cell parameter (Å) ($\pm 3 \times 10^{-3}$ Å)	Particle size (Å) (±5%)	Specific surface (m^2/g)	Integral pore volume (cm^3/g) (±3%)	Micropore volume (cm^3/g) (±50%)	Mean pore diameter (Å) (±5%)
Ca	3.3	10.23	8.0	180	0.41	0.0008	90
Sr	3.1	10.24	7.5	170	0.35	0.0015	80
Ba	2.7	10.25	7.0	160	0.30	0.0019	80

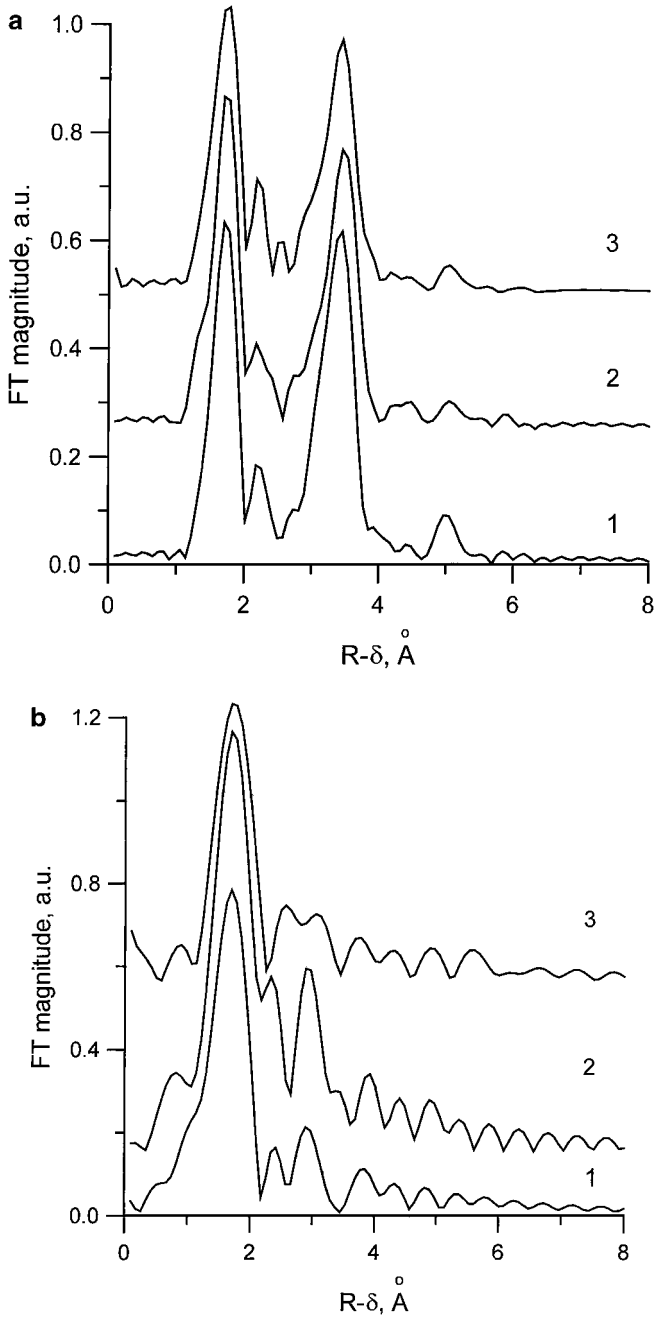

FIG. 2. (a) Typical RDA functions for ZrK edge for bulk mesoporous zirconia supports stabilized by Ca (1), Sr (2), and Ba (3). (b) Typical RDA functions for CuK edge in 5% $CuO/MeO–ZrO_2$ samples with supports stabilized by Ca (1), Sr (2), and Ba (3).

(Table 1). The pore structure is nearly exclusively presented by mesopores with sizes comparable with those of zirconia particles. Hence, mesopores appear to be formed by packing of zirconia particles. The size of mesopores and integral pore volume slightly decrease in the order Ca > Sr > Ba. Only a small fraction of micropores is observed in samples. Though the error in determining small volumes of micropores by standard Brockhoff and de Boer method is rather high (±50%), the amount of micropores is certainly bigger for Ba-containing sample.

2. Structural Features of Supported Systems

No variation in the particles appearance was observed by TEM after supporting CuO using the methods described above.

According to EXAFS data (Fig. 2b; Table 2), for all copper-containing samples, nearly identical square-planar coordination of copper cations by the four oxygen atoms situated at 1.99 Å distance is realized. In general, the next distance (ca. 3 Å) is close to values typical for Cu–Cu distance in copper oxidic clusters [13], though a similar value is observed for Cu–Zr distance in the case of copper cations incorporated into the surface layer of zirconia [14]. To clarify the situation, this peak was modeled by Cu (Cu–Cu sphere) and Zr (Cu–Zr sphere) scattering atoms. The best uncertainty factor (*R* factor) was obtained for Cu–Zr distances, though up to 30% of Cu–Cu distances may also contribute to this peak. Hence, a part of copper cations is certainly incorporated into the surface vacancies of zirconia. At a high copper loading, EXAFS data could not exclude the presence of copper oxidic clusters. At least these results

TABLE 2

Some EXAFS Parameters

Sample	Coordination sphere	Coordination No.	Distance (Å)	Debye-Waller factor $2\sigma^2$ ($Å^2$)
$CaO–ZrO_2$	Zr–O	3.8	2.10	0.010
	Zr–Zr	6.4	3.66	0.016
$SrO–ZrO_2$	Zr–O	4.3	2.11	0.011
	Zr–Zr	5.1	3.67	0.015
$BaO–ZrO_2$	Zr–O	3.8	2.11	0.010
	Zr–Zr	5.1	3.67	0.017
0.2%CuO/ $CaO–ZrO_2$[a]	Cu–O	3.8	1.97	0.016
5%CuO/ $CaO–ZrO_2$[b]	Zr–O	3.9	2.10	0.010
	Zr–Zr	5.4	3.65	0.015
	Cu–O	3.1	1.97	0.010
	Cu–Zr	0.4	2.94	0.016
2%CuO/ $SrO–ZrO_2$[a]	Cu–O	2.8	1.92	0.006
5%CuO/ $SrO–ZrO_2$[b]	Zr–O	3.8	2.10	0.010
	Zr–Zr	5.5	3.66	0.018
	Cu–O	2.9	1.98	0.011
	Cu–Zr	0.5	2.93	0.017
0.2%CuO/ $BaO–ZrO_2$[b]	Cu–O	2.9	1.93	0.004
5%CuO/ $BaO–ZrO_2$[b]	Zr–O	3.9	2.10	0.013
	Zr–Zr	4.5	3.66	0.016
	Cu–O	3.0	1.98	0.011
	Cu–Zr	0.5	2.92	0.017

[a] Ion exchange.
[b] Consecutive impregnation.

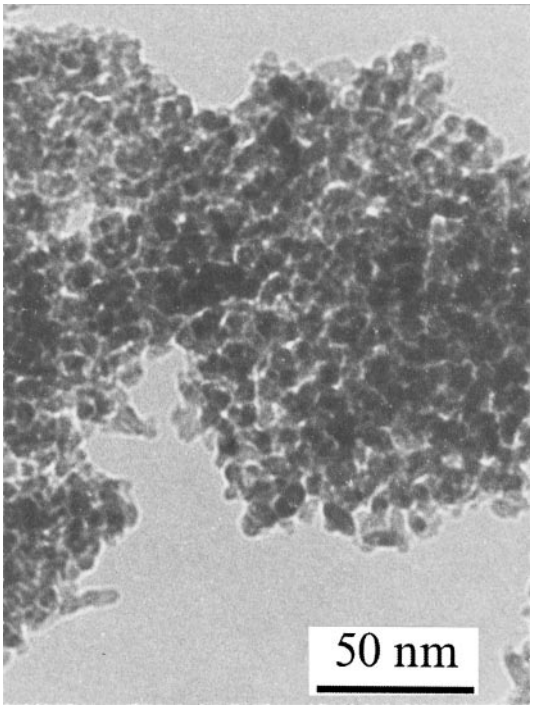

FIG. 3. Typical TEM picture of mesoporous MeO–ZrO_2 support.

agree with the absence of bulk CuO phase as follows from the data of TEM and XRD.

EXAFS spectra of silver not shown here for brevity were found to have a very high noise level, suggesting that supported Ag mainly exists as isolated cations with a low Ag–O coordination number. Certainly, a small part of Ag is present as rather big particles with typical sizes up to 200–400 Å revealed by TEM (Fig. 4). Similar particles were detected by TEM for alumina-supported Ag–Cu system (Fig. 5). Simultaneously, SAXS data (Fig. 6) indicate that a

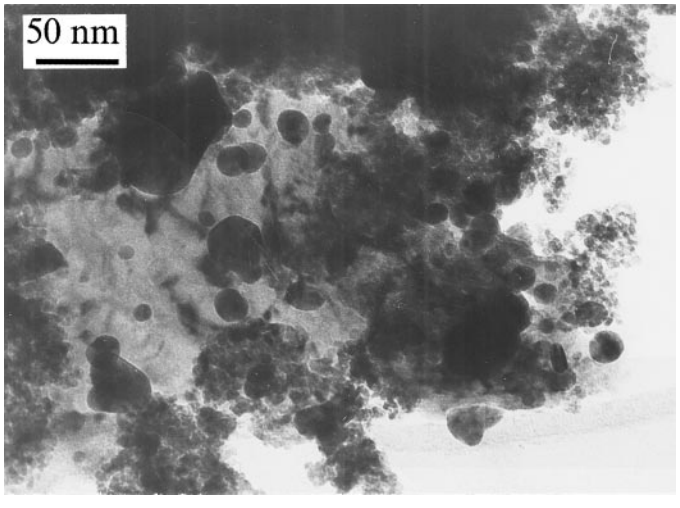

FIG. 4. Typical TEM picture of 2%Ag + 5%CuO/Sr–ZrO_2 sample.

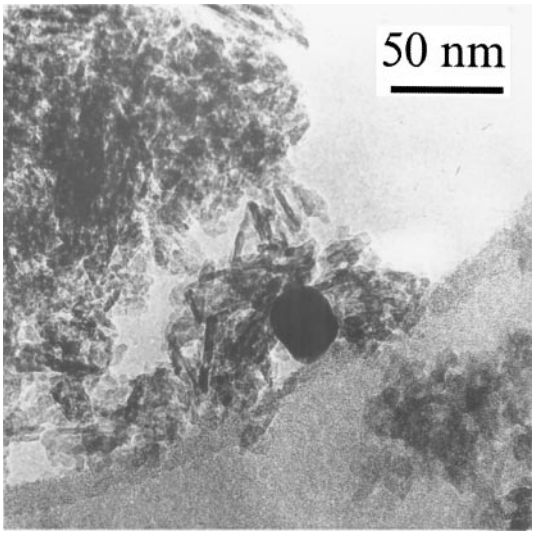

FIG. 5. TEM micrograph of silver particle on the surface of 0.8% Ag + 0.8% CuO/Al_2O_3 sample.

predominant part of silver particles detected by this method are of a rather small sizes confined in the range of 10–20 Å.

For Ag-promoted CuO/stabilized ZrO_2 samples prepared via the impregnation route, the interaction between metallic and oxidic components is manifested in the appearance of thin transparent layers extended around bulk silver particles (Fig. 7). For barium-stabilized zirconia, this interaction is the most strong leading to emergence of thin disordered platelets probably corresponding to mixed copper–silver oxidic phases containing also some Ba (Fig. 8).

Hence, a main part of silver in supported samples is represented by isolated cations incorporated into the support surface layer or copper oxidic species; a small part exists as nanosized particles detected by SAXS, while big particles detected by TEM constitute a negligible fraction of silver.

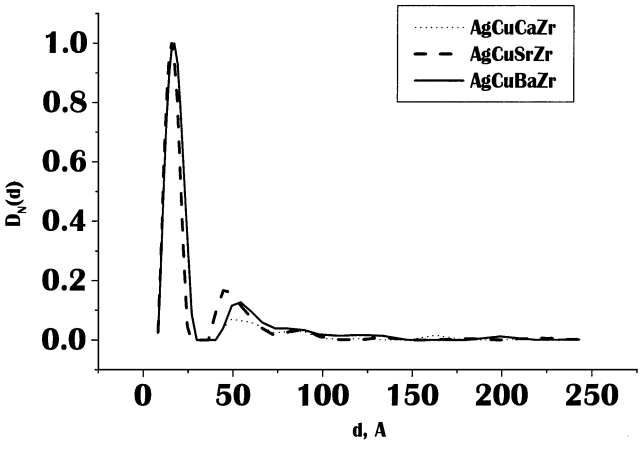

FIG. 6. Normalized SAXS size distribution curve for Ag particles on CuO/stabilized ZrO_2 samples.

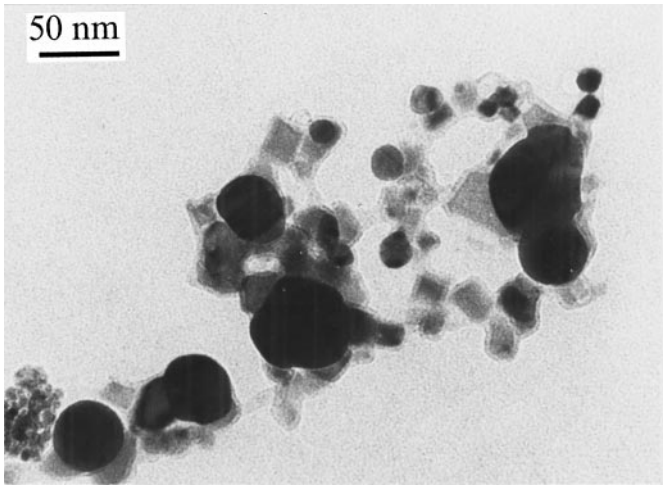

FIG. 7. TEM image of the products of interaction (thin platelets) between silver (dark bulky particles) and copper oxidic species supported onto $CaO–ZrO_2$ sample.

3. IR Spectroscopy of Adsorbed CO

Table 3 lists assignment of CO absorption bands detected for samples studied here. Figures 9 and 10 show typical spectra of CO adsorbed on alumina-supported copper oxidic species. At low temperatures, bands at ~2180–2190 cm^{-1} correspond to CO complexes with isolated Cu^{2+} cations, while bands in the range of 2118–2150 cm^{-1} are due to Cu^{1+}–CO species (15). Reduced copper species emerge either due to oxygen loss from the surface during vacuum pretreatment or due to reduction of clustered copper cations by CO even at low temperatures. Domination of clustered copper species (three-dimensional oxidic clusters (15)) for these samples is suggested by rather low-frequency position of Cu^{1+}–CO band (~2118 cm^{-1} at full coverage).

TABLE 3

Assignment of Carbonyl Bands Observed for Zirconia and Alumina Supported Samples after CO Adsorption at 77 K

Band position (cm^{-1})	Type of center	Reference
2090–2110	Ag^+ in partially oxidized Ag particles	16, 18
2090–2125	Cu^+ in 3D copper oxidic clusters	15
A pair of bands 2090 + 2125	Cu^+, dicarbonyl complexes	21
2140	Ba^{2+} ($BaO-ZrO_2$)	8
2140	Cu^+ in 2D copper oxidic clusters on γ-Al_2O_3	15
2155	Hydroxyls	15
2170–2180	Ag^+ isolated	17
2180–2190	Cu^{2+} isolated	15
2180–2200	Zr^{4+}	8

The frequency shift of this band with increasing coverage (~12 cm^{-1}) is similar in magnitude to that observed in the case of supported metals (16). The clearly visible maximum at ~2140 cm^{-1} in the spectrum recorded after the first dose of CO can be assigned to Cu^+ cations in two-dimensional copper oxidic clusters epitaxially bound with the most developed (110) faces of γ-alumina support (15). The band at ~2155 cm^{-1} well developed in the presence of CO in the gas phase is usually assigned to weak CO complexes with hydroxyls of the support (15). A sample prepared by using photodeposition from the copper acetate solution, despite a higher copper content, is characterized by a lower intensity of Cu^+–CO and Cu^{2+}–CO carbonyl bands as compared with sample prepared by a simple impregnation with copper nitrate solution. It implies a higher degree of copper clustering in the former case.

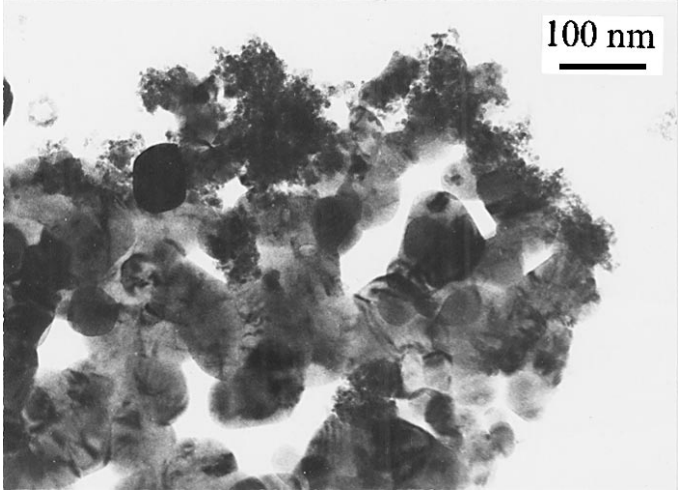

FIG. 8. Typical TEM images of the microphases of interaction between the copper oxide component and silver supported on $BaO–ZrO_2$.

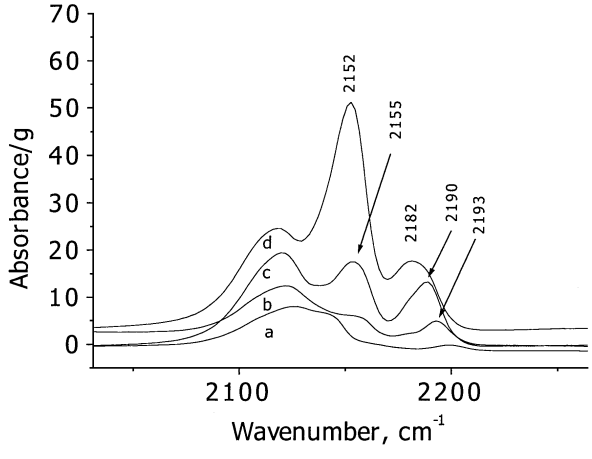

FIG. 9. FTIR spectra of CO adsorbed at 77 K on 0.5% CuO/Al_2O_3 sample prepared from copper nitrate. Spectra were recorded after consecutively introducing into the cell 1 (a), 4 (b), and 9 (c) doses of CO (each dose corresponds to ~4 μmol), finally setting CO pressure to 10 Torr (d).

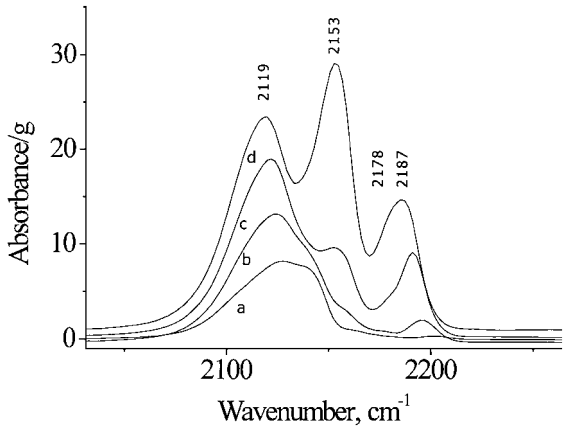

FIG. 10. FTIR spectra of CO adsorbed at 77 K on 0.7%CuO/Al_2O_3 sample prepared from copper acetate. Curves designation as in Fig. 9.

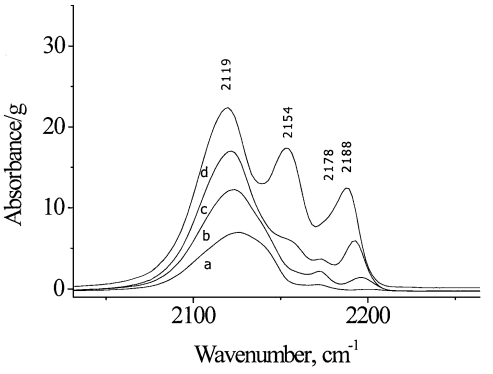

FIG. 12. FTIR spectra of CO adsorbed at 77 K on 0.6% Ag+ 0.7%CuO/Al_2O_3 sample prepared from copper acetate. Curves designation as in Fig. 9.

For copper–alumina samples promoted by silver (Figs. 11 and 12), after several doses of CO weak bands at 2170–2180 cm^{-1} appear. These bands can be assigned to Ag^+–CO complexes (17). At higher coverages, these bands are masked by broad bands corresponding to weaker CO complexes with hydroxyls and Cu^{2+} cations. Decline of the intensity of band at ~2152 cm^{-1} for silver-modified samples implies that these silver cations are anchored through the ion exchange with hydrogen of these hydroxyls.

For samples prepared from copper nitrate, the presence of silver only slightly affects the spectral features of CO complexes with copper cations: a shoulder at ~2110 cm^{-1} is now visible in spectrum recorded after the first dose. It implies that a part of silver supported through the photoassisted deposition is located on the copper oxidic clusters changing their properties. However, the integral intensity of Cu^+–CO band in the presence of CO in the gas phase was practically unchanged for silver-promoted sample. Hence, this feature can be assigned to CO species located on the surface of partially oxidized Ag° particles. Indeed, for bulk silver the band corresponding to Ag°–CO species is observed at ~2060 cm^{-1} (18). The high-frequency shift of Ag°–CO band can be explained either by CO adsorption on high index planes abundant on small silver particles or by dynamic and/or chemical effects due to the presence of adsorbed oxygen on the surface (16). Hence, in this case, silver particles and copper oxidic species appear to be independently distributed on the surface of alumina support.

In the case of samples prepared from acetate, the effect of silver photodeposition was much more pronounced. First, the intensity of Cu^+–CO and Cu^{2+}–CO bands declines for silver-promoted sample, indicating that at least some of the silver particles are juxtaposed on copper oxidic species. Further, in the spectrum recorded after the first CO dose, a shoulder at ~2140 cm^{-1}, corresponding to CO adsorbed on Cu^+ cations included in two-dimensional oxidic clusters disappears. Hence, small silver particles appear to be mainly located on neighboring copper cations situated at the most developed (110) alumina surface planes.

CO adsorption on the surface of stabilized zirconia supports revealed rather strong adsorption centers—coordinatively unsaturated Zn^{4+} cations (bands at ~2180–2190 cm^{-1}). After the first CO dose, a weak shoulder at ~2140 cm^{-1} which can be tentatively assigned to CO complexes with Me^{2+} cation is observed only in the case of Ba-containing sample (Fig. 13a). As was discussed earlier (8), it implies mainly the subsurface location of guest cations. At low CO coverages, the intensity of Zn^{4+}–CO bands only slightly depends upon the nature of the system, suggesting a comparable number of strong Lewis acid sites (Fig. 13a). In the presence of CO in the gas phase, a broad band with the maximum at ~2155 cm^{-1} (CO adsorbed on surface hydroxyls) and a shoulder at ~2180 cm^{-1} (Zn^{4+}–CO complexes) are observed (Fig. 13b). The surface concentration of hydroxyls is certainly higher for the Ba–Zr system. While for Ba–Zr and Sr–Zr systems the high-frequency

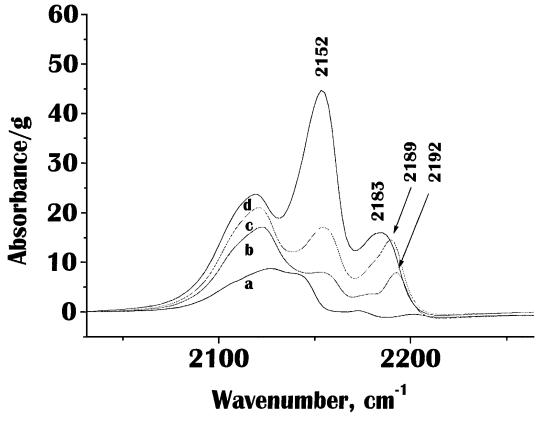

FIG. 11. FTIR spectra of CO adsorbed at 77 K on 0.3% Ag+ 0.5%CuO/Al_2O_3 sample prepared from copper nitrate. Curves designation as in Fig. 9.

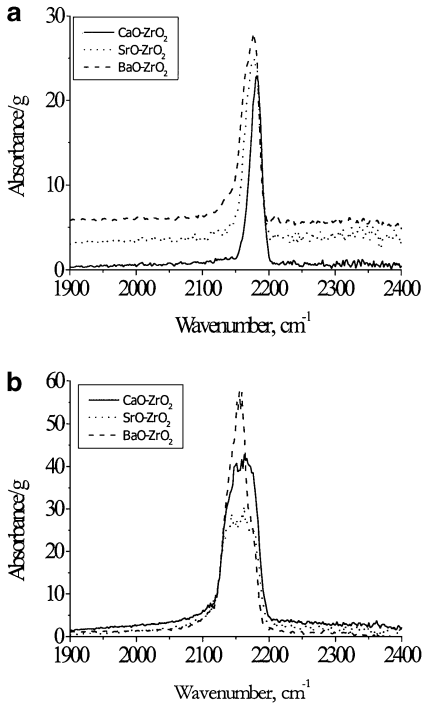

FIG. 13. FTIR spectra of CO adsorbed at 77 K on stabilized mesoporous zirconia samples. (a) First dose of CO; (b) 10 Torr of CO.

absorption corresponding to Zn^{4+}–CO complexes appears to be saturated even after the first dose, it does increase with CO pressure for Ca–Zr sample, indicating, the existence of a weaker Lewis acid site.

For samples with a low copper content (Fig. 14), along with bands at 2180–2190 cm^{-1} corresponding to Zn^{4+}–CO and Cu^{2+}–CO complexes, new bands, which can be tentatively assigned to CO complexes with clustered Cu^{1+} cations, appear in the 2115–2125 cm^{-1} region. Hence, along with isolated Cu^{2+} cations incorporated into the surface layer of the support (corresponding band at ~2180–2190 cm^{-1} is superimposed with Zn^{4+}–CO band), some copper cations seem to be present as small clusters. As judged only by the Cu^{+}–CO band position, at low copper loading, the degree of copper cation clustering appears to be somewhat higher in the case of stabilized zirconia support when compared with alumina (Figs. 9 and 10). However, the situation could be much more complex, since, according to (7, 19–22), for fluorite-type supports, even isolated surface Cu^{2+} cations can be easily reduced by CO at low temperatures to Cu^{+} and/or Cu° state, thus giving rise to low-frequency carbonyl bands, while in the case of alumina support, only small three-dimensional clusters possess such properties.

For the $BaO–ZrO_2$ system, a higher intensity of Cu^{+}–CO band at a low (0.1 Torr) CO pressure indicates a higher surface concentration of coordinatively unsaturated Cu^{+} cations as compared with the other two samples. This feature clearly correlates with a higher density of surface hydroxyls on the surface of this support (vide supra) and a higher degree of sample disordering (lower X-ray particle sizes). At higher CO partial pressures, for the $BaO–ZrO_2$ system, the initial band at 2115 cm^{-1} is split into two bands at 2090 and 2125 cm^{-1}, corresponding to copper dicarbonyl species (23). This suggests the highest degree of coordinative unsaturation of copper cations for this support. A feature at ca. 2140 cm^{-1} for $BaO–ZrO_2$ based sample observed at $p\mathrm{CO} = 10$ Torr can be assigned to CO complexes with Ba cations (vide supra).

An increase in the copper loading on stabilized zirconia supports (Fig. 15) was accompanied by a decline in the normalized (per gram) intensity of all carbonyl bands in the 2000–2200 cm^{-1} region. Coordinatively unsaturated Zn^{4+} cations appear to be completely shielded by the copper oxidic species. Bands corresponding to Cu^{+}–CO complexes are red shifted, indicating a higher degree of copper cation clustering (aggregation) (15). The higher the degree of clustering in the order $CuO/BaO–ZrO_2 > CuO/SrO–ZrO_2 > CuO/CaO–ZrO_2$, the lower the band intensity and corresponding CO stretching frequency. At the same copper content, the clustering degree appears to be mainly determined by the specific surface area and amount of micropores (Table 1). At a high CO pressure (Fig. 15b), a band at ~2155 cm^{-1} emerges due to CO complexes with hydroxyls, its intensity being lower than with the case of initial

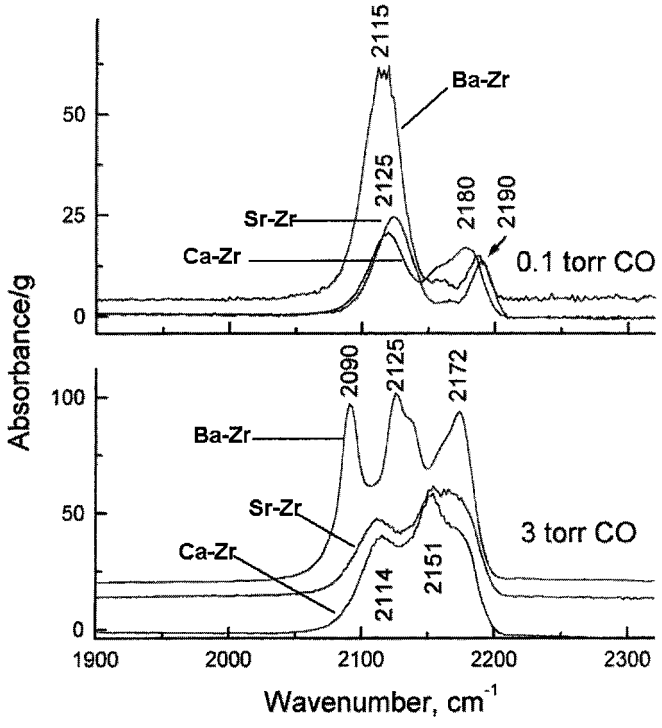

FIG. 14. FTIR spectra of CO adsorbed at 77 K on samples of stabilized mesoporous zirconia containing 0.2 wt% of Cu introduced via cation exchange. (Top) 0.1 Torr CO; (bottom) 3 Torr CO.

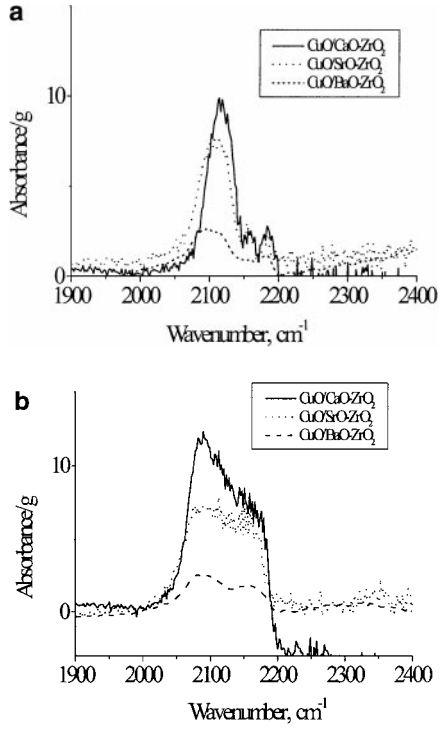

FIG. 15. FTIR spectra of CO adsorbed at 77 K on samples of stabilized mesoporous zirconia containing 5 wt% of Cu introduced by impregnation. (a) First dose of CO; (b) 10 Torr of CO.

supports (cf. Fig. 13). Hence, both Lewis and Brönsted acid sites take part in anchoring the surface copper species.

For samples prepared via the successive photoassisted deposition of copper and silver (vide supra), FTIRS data of adsorbed CO (Figs. 16–18) strongly resemble those for the

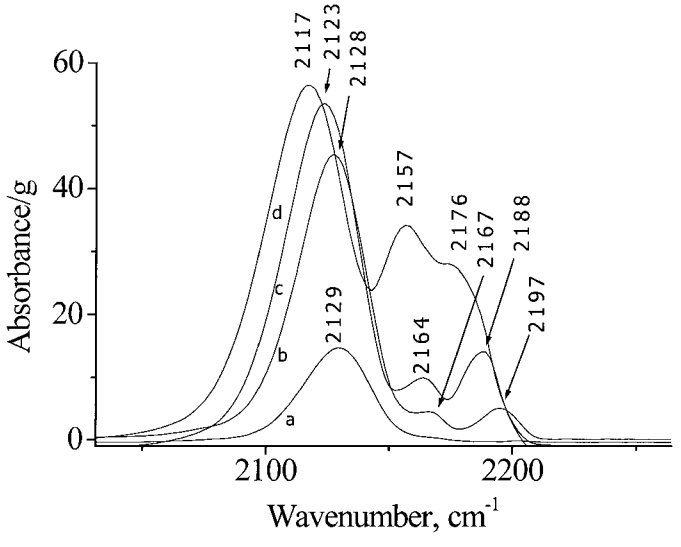

FIG. 16. FTIR spectra of CO adsorbed at 77 K on sample containing 0.2% Ag + 3.1 wt% of CuO loaded by the photoassisted deposition on CaO–ZrO$_2$ support. Curves designation as in Fig. 9.

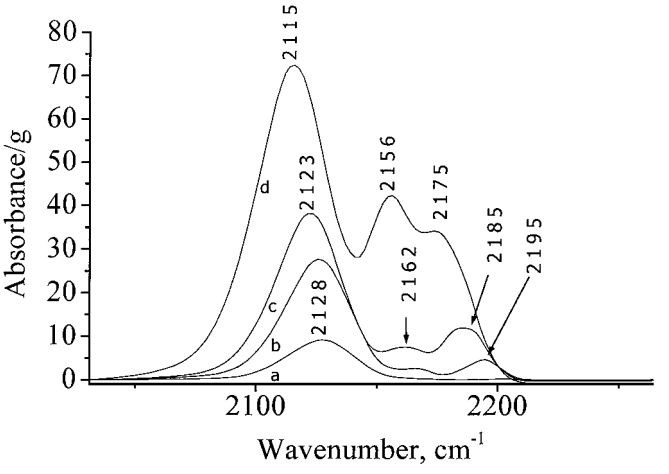

FIG. 17. FTIR spectra of CO adsorbed at 77 K on sample containing 0.2% Ag + 2.5 wt% of CuO loaded by the photoassisted deposition on SrO–ZrO$_2$ support. Curves designation as in Fig. 9.

CuO + Ag/alumina system prepared via the same route. They indicate a lower degree of clustering of copper cations (higher intensity and higher frequency of Cu^+–CO band) compared with systems prepared via the impregnation route. For the 0.8Ag + 3CuO/BaO–ZrO$_2$ sample, a part of Zn^{4+} coordinatively unsaturated centers remains accessible, which is evident from the appearance of a band at ~2190 cm^{-1} after the first CO dose. For this sample, at 10 Torr CO pressure, in the high-frequency carbonyl region, in addition to the usual band at 2155 cm^{-1}, two more maxima at ~2175 and ~2185 cm^{-1} are observed. While the latter band clearly corresponds to Zn^{4+}–CO species (vide supra), the former one can be assigned to Ag^+–CO species. For other two zirconia-supported samples prepared via this route, Ag^+–CO band certainly dominates due to apparently lower surface density of coordinatively unsaturated Zn^{4+}

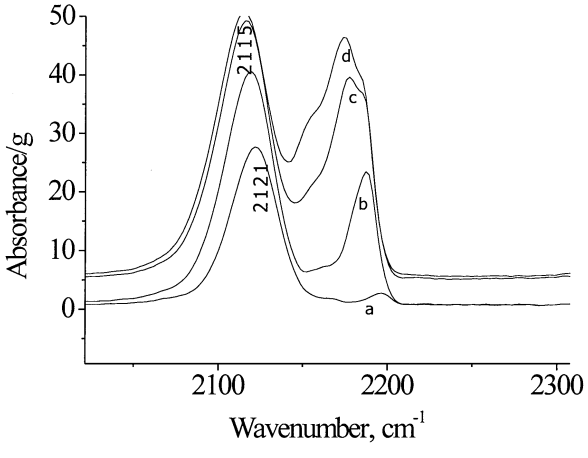

FIG. 18. FTIR spectra of CO adsorbed at 77 K on sample containing 0.8% Ag + 3 wt% of CuO loaded by the photoassisted deposition on BaO–ZrO$_2$ support. Curves designation as in Fig. 9.

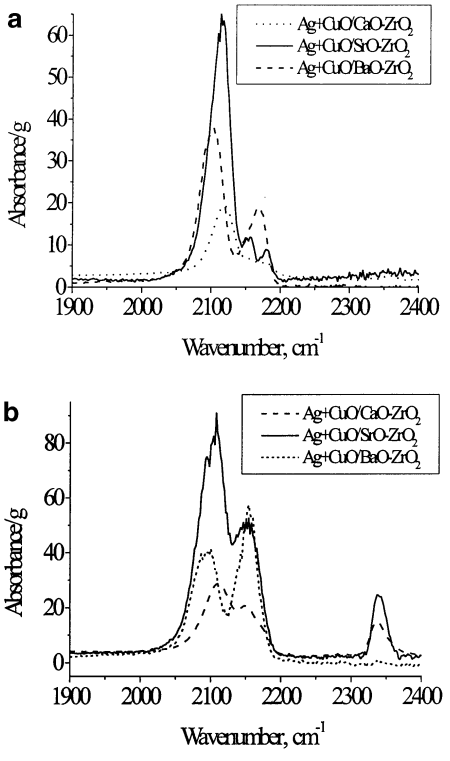

FIG. 19. FTIR spectra of CO adsorbed at 77 K on samples of stabilized mesoporous zirconia containing 2% Ag + 5 wt% of CuO introduced by impregnation. (a) First dose of CO; (b) 10 Torr of CO.

centers. No bands which can be assigned to Ag°–CO complexes are visible in these figures. In the case of zirconia supports as compared with the alumina-supported system (Figs. 11 and 12), a higher absorption at ~2175 cm^{-1} for silver-containing samples implies a higher degree of silver dispersion in the former case.

For samples with higher silver and copper content (Fig. 19) prepared by the impregnation procedure modified to enhance the interaction between the metal and oxidic components (vide supra), a sharp increase in the intensity of Cu^+–CO bands due to Ag addition was observed (cf. Fig. 15). It implies a disordering and/or redispersion of large copper oxidic clusters due to such a treatment. For Sr- and Ba-containing samples, silver addition also causes a red shift of Cu^+–CO absorption band to 2100–2105 cm^{-1} for spectra recorded after the first CO dose (Fig. 19a) and to 2090–2098 cm^{-1} for spectra recorded under 10 Torr of CO (Fig. 19b). This effect implies the existence of CO molecules adsorbed on metallic Ag° species at low temperatures (vide supra). In addition, for spectra recorded after the first CO dose, the appearance of bands at 2170–2180 cm^{-1} implies the presence of CO complexes with coordinatively unsaturated Ag^+–CO species (17). In this respect, for $CaO–ZrO_2$ support, the lowest intensity of these bands as well as the highest frequency and lowest intensity of band in the Cu^+–CO stretching region imply the lowest surface concentration of accessible metallic or ionic silver sites. It can be tentatively explained by a higher aggregation of oxidic and/or metallic species on this support due to its lower disordering (hence, a smaller density of surface defect sites) as demonstrated by the structural data (vide supra). This conclusion is supported by the data in Table 2 which shows higher Cu–O and lower Cu–Zr coordination numbers in the $CaO–ZrO_2$-supported catalyst (Table 2).

Addition of silver strongly enhanced the reactivity of supported copper oxidic species enabling them to oxidize CO at as low a temperature as 77 K with formation of physically adsorbed CO_2 (band at ~2340 cm^{-1}, Fig. 19b). The intensity of this band varies from sample to sample apparently correlating with the amount of reactive weakly bound oxygen removed by CO from copper (copper + silver) oxidic species in the course of experiment. This amount is the highest for $2Ag + CuO/SrO–ZrO_2$ sample with the highest intensity of Cu^+–CO ($Ag^{\delta+}$–CO) band corresponding to three-dimensional oxidic clusters and/or microphases of interactions between silver and copper oxidic species (vide supra). For other two samples, CO_2 band is apparently more intensive for $Ag + CuO/CaO–ZrO_2$ sample, for which the intensity of the carbonyl band increases more when going from the first dose to 10 Torr of CO, thus implying a higher degree of that sample reduction in the course of measurements.

4. Temperature-Programmed Desorption of NO_x

Typical TPD data are presented in Figs. 20 and 21. For low-concentrated Cu-supported samples, low-temperature (<100°C) maxima or shoulders on the complex contours of desorption peaks correspond to decomposition of nitrosyl species bound with isolated Cu^{2+} cations (12). Desorption maxima in the range up to 250°C are assigned to nitrite species bound either with copper or Zr cations.

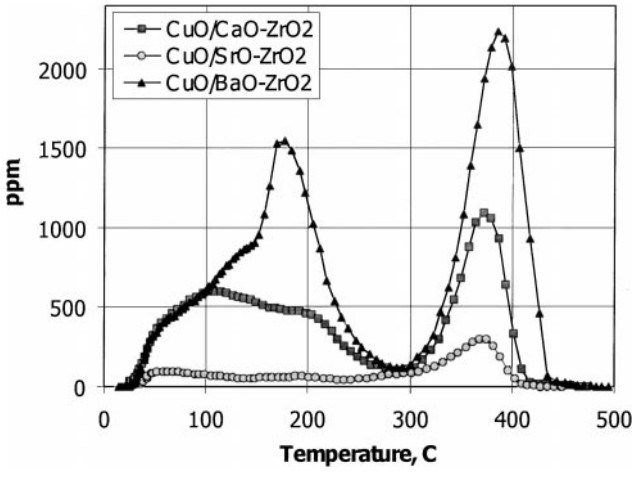

FIG. 20. TPD spectra of NO_x for samples containing 0.2 wt% of CuO introduced via cation exchange on zirconia supports.

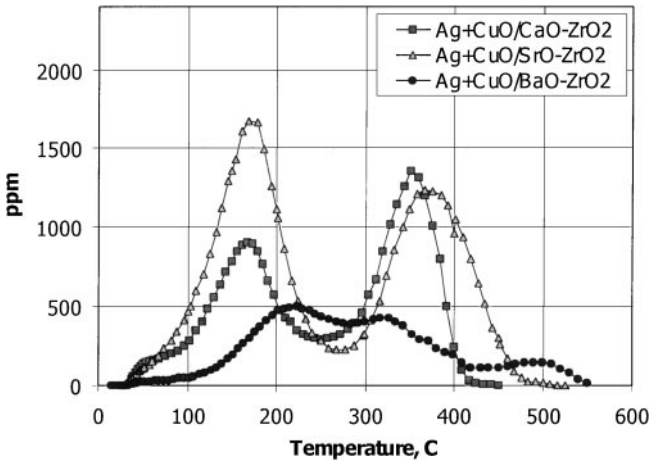

FIG. 21. TPD spectra of NO_x for samples containing 2% Ag + 5 wt% of CuO introduced by impregnation of zirconia supports.

Indeed, TPD maxima at these temperatures were also observed for samples of zirconia partially stabilized by Ca, Sr, and Ba; alumina and CuO/alumina catalysts (12). In the high-temperature region, for CuO/MeO–ZrO_2 samples, T_{max} (~380–390°C) are lower than corresponding values for CuO/alumina (480°C) and partially stabilized zirconias (540–590°C), while being practically identical with that for Cu–ZSM-5 (12). For samples studied here, all peaks are composed of evolved NO molecules, except for CaO–ZrO_2-supported CuO (CuO + Ag) and BaO–ZrO_2 supported CuO + Ag, where the high-temperature peak result from ~10% NO_2 and 90% NO. As was concluded earlier considering FTIRS data on the dynamics of ad-NO_x species transformation in the course of thermal desorption (13), it implies that strongly bound adspecies correspond to nitrates (monodentate and bidentate) rather than nitrites. The integral amount of ad-NO_x species (Table 4) does not exceed several percent of monolayer, suggesting that a predominant part of the surface is free from these species. For samples with a low copper content, in the first approximation, the amount of chemisorbed NO correlates with the density of coordinatively unsaturated surface cations able to adsorb CO (cf. Fig. 14). Moreover, the integral amount of adsorbed NO_x species for zirconia support, either partially stabilized (12), or pure monoclinic one (Table 4) is comparable or even higher than in the case of copper-containing systems, thermal stability of strongly bound nitrates species being higher as well.

TABLE 4

Integral Amount of NO Desorbed from the Surface of Samples Pretreated in Oxygen

	0.2%Cu			2% Ag + 5%Cu			
Sample	CaZr	SrZr	BaZr	CaZr	SrZr	BaZr	ZrO_2^a
a_Σ (10^{19} molec/g)	5.8	1	11	5.8	7.1	2.5	12 (T_{max} 90°C; 440°C)

[a] Sample prepared by the same procedure as other supports without addition of surfactants and alkaline-earth cations. Specific surface 100 m^2/g, 50% cubic + 50% monoclinic phase.

The increase of the copper content and addition of silver have not appreciably affected the level of NO chemisorption for CaO–ZrO_2-based samples, whereas large effects are apparent for the Ba- and Sr-containing systems (Table 4). In general, for silver-containing samples, no simple correlation between the integral amount of adsorbed NO_x and intensity of bands corresponding to CO adsorbed at different centers (cf. Fig. 19) can be derived. In part, this can be explained by a variety of ad-NO_x forms located at chemically different centers as well as by the difficulty in estimation the surface centers concentration from the optical density of overlapping bands corresponding to CO complexes with different absorption coefficients (15). Furthermore, while CO is more strongly bound with Cu^{1+} cations, thus ensuring domination of corresponding bands in the carbonyl region, nitrite and nitrate species are strongly bound with Cu^{2+} cations often completely shielded by oxygen to CO adsorption (15). Nevertheless, some qualitative conclusions can be obtained by considering this data. Thus, an apparent shift of low-temperature peaks to higher temperatures due to silver addition suggests some strengthening of nitrites or monodentate nitrates bonding with the surface. On the contrary, high-temperature peaks are certainly shifted to lower temperatures. It implies some decrease of bonding strength and stability of bidentate or bridging nitrates, which can be tentatively assigned to the replacement of some of the Cu^{2+} cations by Ag^+ cations with a lower effective charge, and, hence, low ability to retain negatively charged NO_3^- group (12). All these features are clearly indicative of the non-additive behavior of mixed supported copper-silver oxidic systems. Indeed, in the case of Ag-ZSM-5 sample (77% exchange level), two NO_x TPD maxima at ~140 and 380°C were earlier observed (11), which clearly could not explain the shift of TPD maxima caused by addition of silver- to copper-supported systems revealed in our experiments.

Appearance of high-temperature TPD maximum for Ag + CuO/BaO–ZrO_2 samples can be assigned either to nitrates bound with Ba cations (12), bulk-like silver nitrite species (10), or to decomposition of the surface $AgNO_3$ phase (24).

DISCUSSION

1. Effect of Support

In general, the mesoporous stabilized cubic zirconia (CaO–ZrO_2, SrO–ZrO_2, and BaO–ZrO_2) supports

synthesized and studied here possess rather similar bulk, surface and textural properties. Hence, at the level of zirconia doping used in the present work and for the Ca- and Sr-containing systems, the surface layer rearrangement into the perovskite-like structure leading to the anion vacancies and Lewis acid centers disappearance (8) does not take place. As a result, at the same doping level of different alkaline-earth cation, the number and strength of Lewis acid sites are comparable. Nevertheless, a somewhat higher tendency of bulky Ba cation to segregate in the surface layer (8) is reflected in a higher degree of the surface disordering and higher concentration of hydroxyls able to weakly interact with CO at low temperatures. Due to this enhanced surface reactivity, Ba-doped mesoporous zirconia is slightly less stable toward sintering, which is reflected in a lower surface area and increased microporosity. For this system, at a low level of copper loading, copper cations are highly coordinatively unsaturated, thus being able to form dicarbonyls and retain a considerable amount of ad-NO_x species.

In contrast to such traditional supports as γ-alumina, stabilized zirconia supports appear to favor formation of small reactive (probably, three-dimensional) clusters of copper cations possessing a decreased strength of oxygen bonding with these centers, and, hence, increased reactivity. In our case, it is reflected in decreased thermal stability of surface nitrate species located at these centers as compared with such species on the surface of CuO/alumina catalysts. This feature seems to be primarily determined by the specificity of the surface structure of fluorite-like supports (ceria, zirconia). In general, for those supports, as was found here in agreement with previous studies (7, 21, 22), the increase of copper loading was shown to be accompanied by the progressive clustering of copper cations into oxidic species. Such species can be termed as 3D metastable oxidic clusters. As revealed by oxygen TPD data (21, 22), up to a certain degree of loading dependent upon the specific surface area of support and its chemical composition, a higher clustering degree results in lower strength of oxygen bonding with copper cations. The shift of CO and H_2 TPR peaks to lower temperatures with the increase of clustering degree (21, 22) proves that weakly bound oxygen is indeed reactive species. At a certain level of copper loading (usually, in the range of 10–15 wt%), bulky oxidic particles with a structure resembling that of CuO, and, at last, X-ray detected CuO phase appear (7). Those species are characterized by TPD and TPR peaks situated at higher temperatures as compared with the peaks observed for the case of low-concentrated copper–zirconia samples or even bulk CuO (7, 21, 22).

Earlier obtained estimations of the heats of oxygen adsorption on different types of copper centers in copper-supported systems (15) make it possible to understand this data taking into account specificity of the structural arrangement of various copper species. For isolated copper cations inserted into the vacant positions of a support surface, the surface oxygen form is characterized by the heat of oxygen desorption ca. 110–120 kJ/mol. For the most developed (110) plane of alumina support, epitaxially bound 2D copper oxidic clusters are covered by tightly bound bridging oxygen forms with the heat of desorption in the range of 290 kJ/mol. Due to steric reasons, only boundary copper atoms in 2D clusters can be covered by terminal (Cu-O) oxygen forms. Bridging oxygen forms with a similar high heats of desorption cover the most developed densely packed faces of tenorite (CuO) particles, provided that surface defects are absent. For 3D metastable oxidic clusters such as those stabilized by fluorite-like supports, due to steric hindrances, surface is to be covered by terminal (Me-O) oxygen forms. Moreover, due to structure rearrangement caused by removal of oxygen from the surface, namely, formation of relatively strong Cu–Cu bonds, compensating in such a way a part of energy spent by the rupture of the Cu–O bond, the heat of oxygen desorption is additionally decreased up to 20 kJ/mol (14). Up to a certain limit, for fluorite-like supports, the increase of copper loading increases the size of 3D clusters, which is to be accompanied by the decrease of the share of the surface copper cations accessible to CO adsorption, which is indeed observed (vide supra). Moreover, for a bigger cluster, its structure relaxation caused by the oxygen removal is to be more pronounced, thus decreasing a mean values of the copper–oxygen bonding strength and increasing its reactivity, which agrees with the experimental data (7, 21, 22).

Hence, enhanced low-temperature performance of copper–zirconia systems in the NO_x selective reduction by hydrocarbons (1–6) can in part be assigned to the specificity of fluorite-like supports surface structure affecting the strength of oxygen bonding with isolated/clustered copper oxidic species, which is important from the point of view of reactants activation.

2. Effect of Silver

The effect of silver seems to depend upon the type of support and preparation procedure. In the case of consecutive photoassisted deposition, the adsorption properties of supported copper oxidic species are only moderately affected by silver. As can be judged from the results obtained with alumina support, silver particles appear to be preferentially photodeposited upon associates of copper cations or copper oxidic clusters epitaxially bound with support, thus decreasing the surface density of coordinatively unsaturated copper cations.

In the case of the consecutive impregnation procedure followed by a partial acid dissolution of supported species with subsequent reprecipitation as described under methods, the interaction between silver and copper is very strong, allowing formation of mixed phases revealed as separate micro-phases. As a result, the adsorption properties of

supported copper oxidic species are strongly modified due to possible appearance of Ag atoms as next-nearest neighbors in the coordination sphere of copper. As a result, the reactivity of surface oxygen is certainly enhanced which is reflected in very efficient oxidation of adsorbed CO even at 77 K.

3. Nature of ad-NO_x Species

For zirconia-supported copper oxidic species including those promoted by silver, TPD data revealed ad-NO_x species with thermal stability and strength of bonding comparable with those in Cu-ZSM-5, which can be assigned to nitrosyls (weakly bound species) and monodentate/bidentate nitrates (strongly bound species). Taking into account conclusions about participation of strongly bound nitrates in the reaction scheme of HC-NO_x SCR (10, 12–14), these results seem to explain a comparable performance of Cu/ZrO_2 and Cu-ZSM-5 systems in these reactions. A weakening of the metal–oxygen bond in mixed silver–copper oxidic species can in part be responsible for decreased thermal stability of surface bidentate nitrates.

CONCLUSIONS

Mesoporous samples of high-surface-area zirconia stabilized by alkaline-earth cations synthesized via coprecipitation followed by refluxing in the presence of surfactants were found to possess a cubic structure with a local tetragonal distortion of Zr coordination sphere compensated on average within the oxide crystallites. These supports possess sufficient Lewis and Brønsted acidity to ensure a good dispersion of supported copper and silver species. The effects of interaction between these species and their adsorption properties strongly depend on the synthesis procedure. In contrast to such traditional supports as γ-alumina, stabilized zirconia supports appear to favor formation of small reactive (probably, three-dimensional) clusters of copper cations possessing an increased reactivity and decreased strength of oxygen bonding with these cations. It is reflected in decreased thermal stability of surface nitrite and nitrate species located at these centers as compared with such species on the surface of CuO/alumina catalysts. This feature seems to be primarily determined by the specificity of the surface structure of fluorite-like supports (ceria, zirconia). For samples prepared via the photodeposition route, the clustering degree of copper cations is usually lower than in the case of samples obtained by traditional impregnation procedure due to a more uniform spatial distribution of the active component on support.

The effect of silver on the adsorption properties of supported copper oxidic species depends upon the type of support and preparation procedure. In the case of photo deposition, silver nanoparticles are either juxtaposed upon copper oxidic species, decreasing the number of coordinatively unsaturated copper cations, or independently located on the accessible sites via interaction with surface hydroxyls. In the case of a special consecutive impregnation procedure aimed at enhancing the interaction between copper and silver, silver incorporation into copper oxidic clusters decreases the strength of copper–oxygen bonds as well as thermal stability of adsorbed bidentate and bridging nitrate species.

ACKNOWLEDGMENTS

This work was in part supported by INTAS 97-11720 project.

REFERENCES

1. Bethke, K. A., Alt, D., and Kung, M. C., *Catal. Lett.* **25**, 37 (1994).
2. Bethke, K. A., Kung, M. C., Yang, B., Shah, M., Alt, D., Li, C., and Kung, H. H., *Catal. Today* **26**, 169 (1995).
3. Bethke, K. A., Li, C., Kung, M. C., Yang, B., and Kung, H. H., *Catal. Lett.* **31**, 287 (1995).
4. Figueras, F., Coq, B., Ensuque, E., Tachon, D., and Delahay, G., *Catal. Today* **42**, 117 (1998).
5. Delahay, G., Ensuque, E., Coq, B., and Figueras, F., *J. Catal.* **175**, 7 (1998).
6. Pietrogiacomi, D., Sannino, D., Tuti, S., Ciambelli, P., Indovina, V., Occhiuzzi, M., and Pepe., F., *Appl. Catal. B* **21**, 141 (1999).
7. Kundakovic, Lj., and Flytzani-Stephanopoulos, M., *Appl. Catal. A* **171**, 13 (1998).
8. Sadykov, V. A., Ivanova, A. S., Ivanov, V. P., Alikina, G. M., Kharlanov, A. N., Lunina, E. V., Lunin, V. V., Matyshak, V. A., Zubareva, N. A., and Rozovskii, A. Ya., *in* "Advanced Catalytic Materials" (P. W. Lednor, D. A. Nagaki, and L. T. Thompson, Eds.), Vol. 454, p. 199. Pittsburgh, PA, 1997.
9. Afanasiev, P., Thiollier, A., Breysse, M., and Dubois, J. L., *Topics Catal.* **8**, 147 (1999).
10. Meunier, F. C., Breen, J. P., Zuzaniuk, V., Olsson, M., and Ross, J. R. H., *J. Catal.* **187**, 493 (1999).
11. Li, Zh., and Flytzani-Stephanopoulos, M., *Appl. Catal.* **165**, 15 (1997).
12. Sadykov, V. A., Baron, S. L., Matyshak, V. A., Alikina, G. M., Bunina, R. V., Rozovskii, A. Ya., Lunin, V. V., Lunina, E. V., Kharlanov, A. N., Ivanova, A. S., and Veniaminov, S. A., *Catal. Lett.* **37**, 157 (1996).
13. Sadykov, V. A., Beloshapkin, S. A., Paukshtis, E. A., Alikina, G. M., Kochubei, D. I., Degtyarev, S. P., Bulgakov, N. N., Veniaminov, S. A., Netyaga, E. V., Bunina, R. V., Kharlanov, A. N., Lunina, E. V., Lunin, V. V., Matyshak, V. A., and Rozovskii, A. Ya., *Pol. J. Environ. Studies* **1**, 21 (1997).
14. Sadykov, V. A., Bunina, R. V., Alikina, G. M., Doronin, V. P., Sorokina, T. P., Kochubei, D. I., Novgorodov, B. N., Paukshtis, E. A., Fenelonov, V. B., Derevyankin, A. Yu., Ivanova, A. S., Zaikovskii, V. I., Kuznetsova, T. G., Beloshapkin, S. A. Kolomiichuk, V. N., Plasova, L. M., Matyshak, V. A., Konin, G. A., Rozovskii, A. Ya., Tretyakov, V. F., Burdeynaya, T. N., Davydova, M. N., Ross, J. R. H., Breen, J. P., and Meunier, F. C., *in* "Nanophase and Nanocomposite Materials III" (S. Komarneni, H. Hahn, and J. Parker, Eds.), Vol. 581, p. 435. Warrendale, PA, 2000.
15. Tikhov, S. F., Sadykov, V. A., Kryukova, G. N., Paukshtis, E. A., Popovskii, V. V., Starostina, T. G., Anufrienko, V. F., Razdobarov,

V. A., Bulgakov, N. N., and Kalinkin, A. V., *J. Catal.* **134**, 506 (1992).
16. Sheppard, N., *in* "Vibration Properties of Adsorbates" (E. F. Willes, Ed.), p. 165. Cambridge Proceedings, Springer-Verlag, Berlin, 1980.
17. Hadjiivanov, K., and Knözinger, H., *J. Phys. Chem. B* **102**, 10936 (1998).
18. Wang, X. D., and Greeneer, R. D., *Surf. Sci.* **226**, L51 (1990).
19. Martinez-Arias, A., Fernandez-Garcia, M., Soria, J., and Conesa, J. C., *J. Catal.* **182**, 367 (1999).
20. Indovina, V., Occhiuzzi, M., Pietrogiacomi, D., and Tutti, S., *J. Chem. Phys. B* **103**, 9967 (1999).
21. Luo, M.-F., Zhong, Y.-J., Yuan, X.-X., and Zheng, X.-M., *Appl. Catal. A* **162**, 121 (1997).
22. Zhou, R.-X., Jiang, X.-Y., Mao, J.-X., and Zheng, X.-M., *Appl. Catal. A* **162**, 213 (1997).
23. Braterman, P. S., "Metal Carbonyl Spec." Academic Press, London, 1975.
24. Zemlyanov, D. Yu., Nagy, A., and Schlögl, R., *Appl. Surf. Sci.* **133**, 239 (1998).